Beam Tests of Final Modules and Electronics of the LHCb Outer Tracker in 2005

October 14, 2005

Abstract

This note presents the results of the beam tests of the mass production modules of the LHCb Outer Tracker equipped with final version prototypes of the frontend electronics. The tests were performed in March 2005 at DESY, using a 6 GeV electron beam.

Note

Reference LHCb 2005-076
Date October 14, 2005

Prepared by G.W. van Apeldoorn, Th. Bauer, E. Bos, Yu. Guz[a], T. Ketel, J. Nardulli, A. Pellegrino, T. Sluijk, N. Tuning, P.Vankov, A. Zwart
NIKHEF, Amsterdam, The Netherlands

S. Bachmann, T. Haas, J. Knopf, U. Uwer, D. Wiedner
Physikalisches Institut, Heidelberg, Germany

M. Nedos
University of Dortmund, Germany

[a] On leave from the Institute for High Energy Physics, Protvino, Russia

Contents

List of Figures

1 Introduction

The purpose of these studies was to test the final mass-production modules of the LHCb Outer Tracker (OT) [1, 2] – in combination with the final version of the frontend electronics [3] – in a beam and to determine the main performance parameters of the detector, such as efficiency, coordinate resolution and noise (random and correlated). The dependence of these quantities on the gas gain and the preamplifier threshold is investigated. In addition, they may depend on the beam position along the wire at which the particle crosses the chamber. In order to study these dependencies, the data were taken at various combinations of parameter settings in several beam positions. In total, more than 10^7 events were recorded during the beam test.

The tests were done in March 2005 in the experimental area 22 of DESY at the DESYII accelerator, with an electron beam at energies between 1 and 6 GeV. Most of the data were taken at 6 GeV to minimize multiple scattering, while in order to study multiple scattering effects some runs were taken at lower beam energies.

The OT uses straw tube technology and consists of short modules above

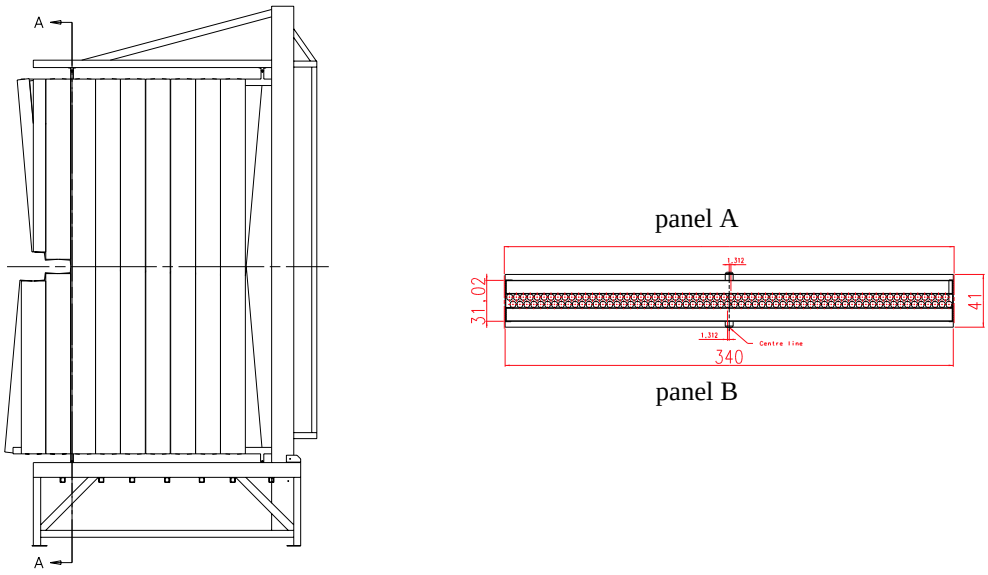

Figure 1: *a) The front view of one half-station of the outer tracker is shown. The short modules that are used in the test are located on the left, above and below the future beampipe. b) The top view of one module is shown. The individual straw tubes are arranged in two mono-layers.*

and below, and of long modules next to the beampipe, respectively, as is shown in Fig. 1a. For the test descibed in this document, four "short" OT modules were used with a length of 2.4 m. One of these short modules consists of two mono-layers (A and B), as is shown in Fig. 1b, and contains 2×64 readout channels. The length of one straw is 2320 mm, the inner diameter of a straw is 4.9 mm, and the straw-to-straw pitch amounts to 5.25 mm.

2 Test Setup

The schematic setup layout is shown in Fig. 2. The test setup comprised four short S1U-type OT modules, consisting of two layers with straws. The complete setup contained a total of eight monolayers, or planes, of straws. Throughout this note the modules and planes will be referred to according to their position along the beam starting from 1, i.e. modules 1–4 and planes 1–8. The chambers were installed in vertical position on a moveable platform. The gas mixture used in these tests was the LHCb baseline gas of 70% Ar and 30% CO_2. Each chamber was equipped with a final prototype frontend box, as is described in Section 3.

The measurement of the detector parameters, such as efficiency and resolution, require knowledge on the coordinate at which the beam particle

	Si			OT							
				M1		M2		M3		M4	
	P1	P2	P3	pl 1	pl 2	pl 3	pl 4	pl 5	pl 6	pl 7	pl 8
Z(mm)	0	267	387	897	902.5	949.5	955	1090	1095.5	1151	1156.5

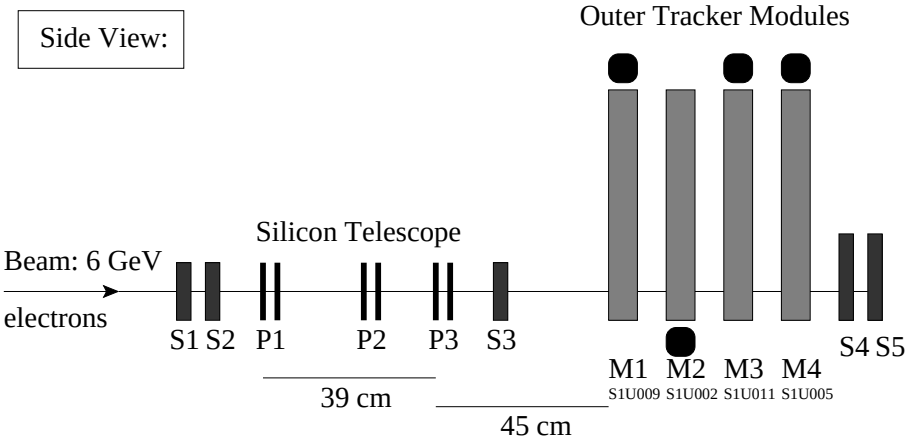

Figure 2: *A schematic picture of the test setup. Note that module 2 is hang upside-down in order to compare the results for particles passing the detector close and far from the frontend electronics.*

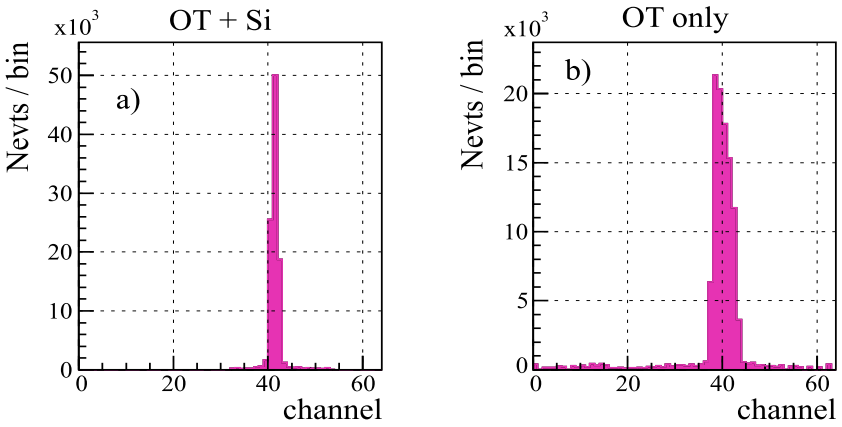

Figure 3: *The OT hit maps for plane 1 (the upstream plane of the first module) are shown with (a) and without (b) the Si-telescope. Note the difference in the number of illuminated straws.*

traverses the detector plane. In order to have a possibility to independently measure track parameters, a silicon strip telescope was used [4]. It consisted of three pairs (X and Y) of 32x32 mm^2, 0.3 mm thick, single sided silicon strip detectors, with 25 μm strip pitch and 50 μm readout pitch. The detectors were mounted inside light tight boxes with 30 μm thick Al windows.

On the other hand, the total number of OT modules (4 modules, or 8 monolayers) were sufficient to reconstruct tracks using OT data only. Therefore part of studies were done without taking Si-telescope data. The trigger signal, which served also as time reference, was produced by coincidence of two scintillator counters S4 and S5 installed downstream of the OT modules. In runs with the Si-telescope included, additional small scintillation counters S1, S2 and S3[1] with a width of 9 mm and a thickness of 2 mm, mounted on the telescope support, were used in coincidence. The beam width in runs with Si-telescope was therefore significantly less than in runs with OT only. The OT hit map is shown in Fig. 3, with (*a*) and without (*b*) the Si-telescope included. In the former case the beam illuminates 2–3 straws per OT plane. When only OT modules were used, several (5–7) straws were fully illuminated. The coordinates and slopes of the tracks measured with the Si-telescope are shown in Fig. 4.

Since the beam was asynchronous with the OTIS chip, unlike in the final experiment at the LHC, in order to measure the OT drift times, the time reference as provided by the scintillators was used. The arrival time of the scintillator signals was measured by the OTIS TDCs and then subtracted

[1]The counter S3 was not used for the most part of data, as it was found to give significant contribution into multiple scattering of beam particles.

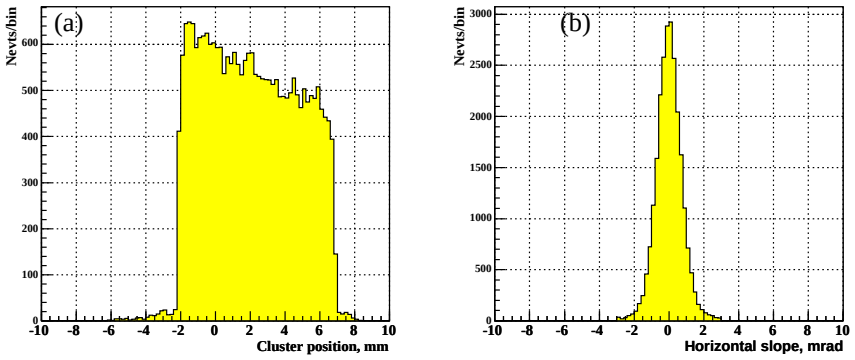

Figure 4: *Beam coordinates (a) and slopes (b) measured by the Si-telescope.*

from the arrival times of the OT signals in order to obtain the drift time:

$$t_{\rm drift} = t_{\rm raw\ TDC} - t_{\rm ref}. \tag{1}$$

More specifically, the average time of S4 and S5 was used as the time reference: $t_{\rm ref} = (t_{S4} + t_{S5})/2$. Its precision, evaluated from the distribution of $t_{diff} = (t_{S5} - t_{S4})/2$, was better than 0.4 ns, see Fig. 5*a*, which is small enough not to affect the OT performance. The raw time distribution of the OT signals is shown in Fig. 5*b*, showing that it fits well into the 75 ns time window of the OTIS. The OT drift time distribution is shown in Fig. 5*c*, showing that the full drift time distribution in these conditions (HV=1600 V) is contained within approximately 42 ns.

In this document the performance of the outer tracker detector and its final frontend electronics will be determined as a function of the high voltage applied, and as a function of the amplifier threshold setting. To a lesser extend, also the dependence on the position of the hit along the straw is estimated.

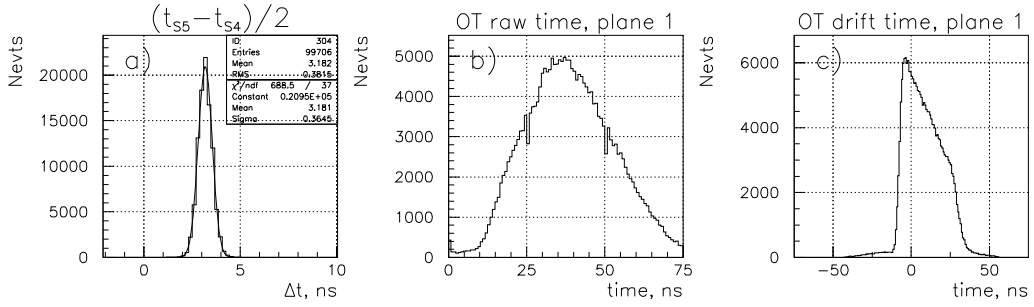

Figure 5: *Precision of the time reference provided by S4 and S5 (a); the arrival time distribution of OT hits (b) and the drift time distribution (c).*

3 The Readout Electronics

Figure 6 shows a schematic overview of the final prototype readout electronics used in the beam test. The on-detector electronics consisted of the amplifiers, TDCs and data serializers housed in one FE-box for each detector (half-) module, and is shown in Fig. 7.

Eight channel amplifiers ASDBLR version 2002 [5, 6] amplified, shaped and discriminated the charge pulse. If the pulse lay above a threshold, the amplifier output a digital differential signal used for the time measurement by the Outer Tracker time Information System (OTIS) TDC [7, 8, 9]. Four ASDBLR amplifiers situated on two PCBs were connected to one OTIS TDC.

The 32 channel OTIS TDC measured the time of the discriminated signal from the amplifier with an accuracy of <1 ns. A delay locked loop (DLL) consisting of 64 inverters subdivided the 40 MHz clock period of 25 ns in 64 bins of 390 ps. When an amplifier signal arrived the number of the active bin was converted to a 6-bit drift time and stored to a pipeline memory. A 32 bit header together with 32 drift times of 8 bit each was output for each accepted event. In the test beam OTIS version 1.2 was used, which was proven to be fully functional. One FE-box was modified with three external timing inputs for the scintillators S4 and S5, in order to obtain a time reference with the same TDC.

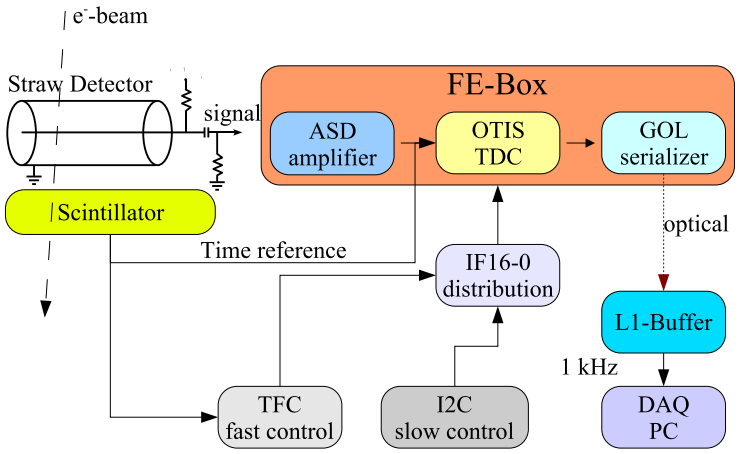

Figure 6: *The beam test readout scheme. Note that the scintillator time reference is specific for this beam test. In the final experiment the L1 buffer will be located in the TELL1 board, and also the DAQ PC will be different.*

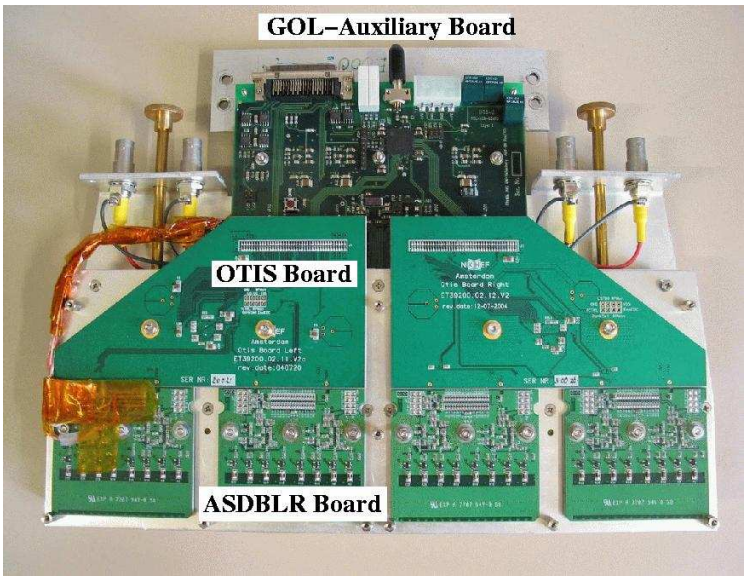

Figure 7: *A photograph of the final prototype front end box.*

Data from four OTIS TDCs, sitting on a separate PCB each, were serialized and 8/10 Bit encoded by a radiation hard Gigabit Optical Link (GOL) chip [10]. The GOL chip output the serial data at 1.6 Gbit/s to a VCSEL laser diode. All 128 channels of one half module were read out over one optical fiber. The GOL chip shares the GOL-Auxiliary-Board [11], with the QPLL [12] clock filter and three low voltage regulators for +3 V, -3 V and +2.5 V.

The optical data was transformed into parallel electrical signals on the optical receiver card (O-RxCard) [13]. The de-serializer on the O-RxCard synchronized the incoming data stream and output the data to a commercial PCI card [14, 15], which employs the same FPGA as the will be used in LHCb, but has a PCI interface. The data was stored on a PC at an event rate of up to 1 kHz allowing high statistic runs.

For the operation of the described readout electronics a fast control system (TFC) and a slow control system (ECS) was necessary in addition. The Timing and Fast Control (TFC) system [16] distributed the 40.0786 MHz LHC clock, L0 decisions, the bunch counter, the event counter[2], plus the reset signals for bunch counter, event counter and L0 electronics optically. The L0 decision was derived from a scintillator coincidence. Different runs were taken either with a coincidence of all five scintillators or with the S4, S5

[2]The event counter counts the L0 accepted events.

scintillators only. For the beam test a local TTC system with a TTCvi [17], TTCvx and a RIO CPU was employed. A TTCrq [18] module mounted on a two output distribution card (IF16-0) received the fast control signals. The TTCrq decoded the serial data and output clock, L0 accept, bunch count reset, event count reset and L0 reset on separate lines. From the IF16-0 service box the TFC signals were differentially lead to the detector modules via 6 m long SCSI2 cables. Slow control settings as amplifier thresholds, OTIS TDC pipeline latency etc. were made via I^2C, running single ended from a PC to the front end boxes.

Throughout the note, the ASDBLR amplifier threshold is expressed in mV as set in practice. The corresponding charge can be obtained to first approximation with:

$$Q(\mathrm{fC}) = e^{-1.25+0.0033\mathrm{Thr(mV)}}, \tag{2}$$

and is shown graphically in Fig. 8:

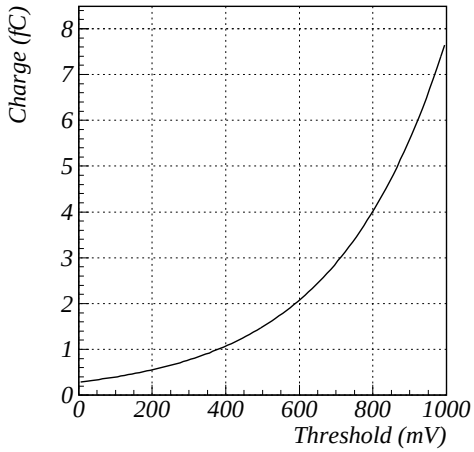

Figure 8: *The approximate correspondance between amplifier threshold and charge is shown.*

4 Analysis

The analysis to estimate the performance of the outer tracker detector and its readout electronics, consist of the following basic steps:

1) Attain the predicted distance of closest approach of the particle to the sense wire.

2) Establish the relation between the measured drift time and the predicted distance to the wire, i.e. the rt-relation.

3) Convert each measured drift time into position coordinate.

With the measured position coordinate in hand, the resolution of this measurement can be obtained by comparing it to the predicted position. The hit finding efficiency is attained by verifying whether the OT produced a hit at the predicted position, within a given window. Three independent analyses have been carried out to estimate the performance of the OT and its readout electronics, and have all used a different method to obtain the rt-relation (also described in [20]). The main differences are listed below, and are given in detail later in this section.

- Track prediction given by the silicon telescope, see Section 4.1.
  - rt-relation is obtained after correcting for the Si-track uncertainty.
  - Efficiency is obtained from the plateau at the center of the cell.
- Track prediction given by the OT, see Section 4.2.
  - The 1^{st} rt-relation is obtained by integrating the TDC spectrum. Subsequently the rt-relation is obtained from a 3^{rd} order polynomial fit to the mean r in slices of the drift time.
  - Efficiency is obtained from the plateau at the center of the cell.
- Track prediction given by the OT, see Section 4.3.
  - rt-relation is obtained iteratively from the track fit.
  - Efficiency is obtained from the average efficiency in a layer. Subsequently a correction for the dead space between the straws is applied.

The procedure of the analyses is explained in this section, whereas the results will be given in Section 6.

4.1 Analysis I: Using Si-telescope for track reconstruction

In studies of the OT modules using the Si-telescope precisely one track per event was required, with a properly reconstructed xz-projection in the telescope. For this, events were selected based on the number of clusters in the Si-detector planes. Exactly one cluster was required in each of the three Si-planes that measure the horizontal coordinate, and 0 or 1 in the planes that measure the vertical coordinate. The total number of clusters had to be equal to 5 or 6. In total 56% of the events passed this cut. An additional cut on the track slopes, $-3 < tx < 3$ mrad and $-3 < ty < 3$ mrad, was applied, see Fig. 4*b*. This cut reduced the number of events by only 3%.

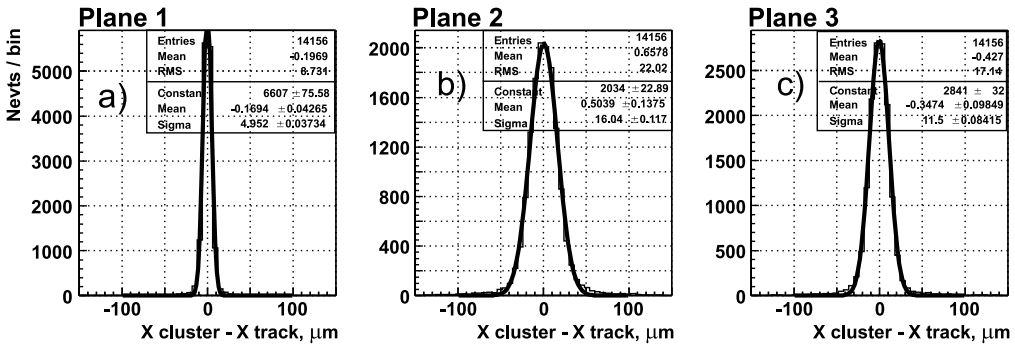

Figure 9: *Distributions of the Si-track residuals in the three Si x planes.*

The intrinsic resolution of the detector planes is better than 3 μm [4]. The width of the distributions of the track residuals is about 5–20 μm, see Fig.9, and is almost fully determined by the multiple scattering in the detector planes. Note that these residuals are biased, since the clusters are used to construct the track. As expected, the middle plane thus has the biggest residual. The residual of the first and third plane differ, because the second

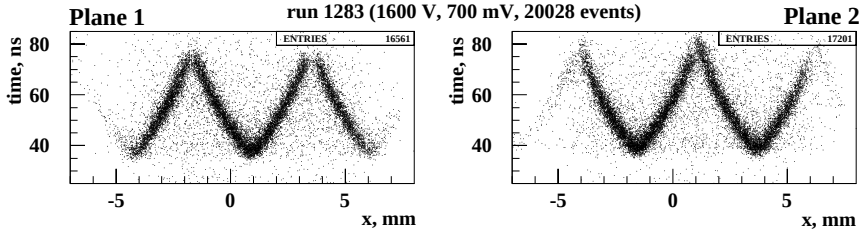

Figure 10: *The drift time vs predicted distance between wire and track reconstructed in the Si-telescope.*

silicon plane is located closer to the third plane than to the first plane.

Figure 10 shows the correlation between the drift time measured in module 1 (planes 1 and 2) and the distance between the wire and the track reconstructed in the Si-telescope. The distinct V-shape patterns expected for drift tubes are clearly seen. The reconstructed Si-track parameters were used to calculate the predicted position $x_{\rm OT}$ for a hit in a plane at $z_{\rm OT}$:

$$x_{\rm OT} = x_{\rm Si,\ P3} + tx_{\rm Si}(z_{\rm OT} - z_{\rm Si,\ P3}), \tag{3}$$

where $tx_{\rm Si}$ is the the slope of the Si-track in the xz-plane. The detector resolution was then extracted from the comparison of the predicted track position with the position as determined from the measured hit, see Appendix A.1.

4.2 Analysis II: OT standalone analysis

Two independent analyses were performed that did not use any information from the silicon telescope, but performed standalone tracking with the OT. The four modules provide potentially eight measurements for a given track, enough for accurate track reconstruction.

In order to estimate the efficiency and resolution, the tracks were reconstructed using the two outer modules only, after which the efficiency and resolution were determined from modules 2 and 3. The effects from noise were minimized by using only those five straws per layer, that were fully illuminated by the beam. Events were selected with good quality tracks by requiring precisely one hit in each layer of module 1 and 4. No cuts are applied on modules 2 and 3.

The raw TDC spectra of each layer differs due to the variation in the delay in the various layers. Figure 11a shows the drift time spectra for all layers, as calculated according to Eq. (1). For each layer a straight line was fitted to the rising edge of the spectrum, after which the TDC time was corrected. This corrected TDC spectrum summed for all layers is shown in Fig. 11b.

An initial rt-relation was obtained by integrating the driftime spectrum [21]. Assuming a uniform illumination of the straw tube the relation between the impact point r of the particle and the corresponding drifttime t can be expressed as:

$$r(t) \ = \ r_{max} \sum_{i=1}^{n} T(t_i),$$

where $T(t)$ denotes the drift time spectrum, normalized to unity, and with r_{max} the straw radius of 2.45 mm. For example, the maximal drift time that contains 25% of all hits, corresponds to $r = 2.45/4$, the maximal drift time that contains 50% of all hits, corresponds to $r = 2.45/2$, and so further.

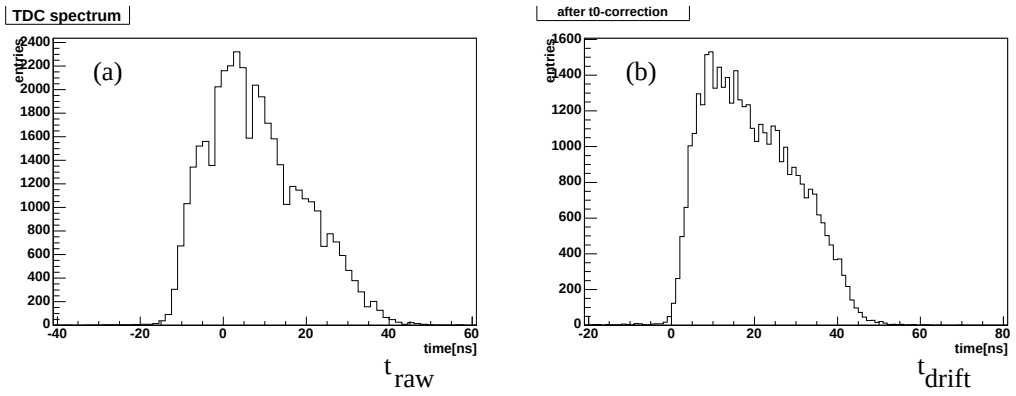

Figure 11: *The TDC spectrum is shown for all layers, before (a) and after t_0-correction. The TDC spectrum corrected for the t_0-correction corresponds to the drift time.*

The measured radius r_{meas} was then calculated for each hit from this initial rt-relation. Subsequently, for each event a straight-line fit of the track was performed, using these hits. The left-right ambiguities were solved by pairing the hits from two neighbouring layers. For the remaining ambiguities a straight line was fitted for all combinations by means of the least square method. These last ambiguities were solved by chosing the solution with the minimal χ^2.

From the resulting rt-distribution as shown in Fig. 12a, a new rt-relation was obtained by slicing the distribution in bins of the drift time. The slices were then fitted with a gauss and their mean values were fitted by a 3^{rd} order polynomial. The resulting rt-relation is shown in Fig. 12b, together with the original rt-relation from the integration of the TDC spectrum.

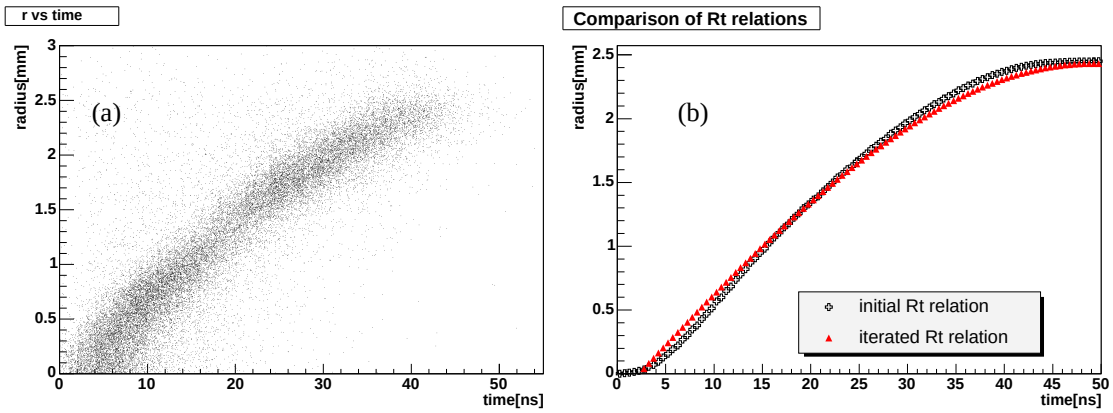

Figure 12: *(a) The relation between the distance to the wire - as obtained from integrating the TDC spectrum - and the drift time is shown. (b) Both rt-relations are shown: the one obtained from integrating the TDC spectrum, and the one obtained from fitting a 3^{rd} order polynomial to time slices of (a).*

4.3 Analysis III: OT standalone analysis

The setup included a total of eight OT straw planes, which is sufficient to reliably reconstruct tracks and estimate the detector characteristics. This OT standalone analysis was performed in exactly the same way as for testbeam results used for the OT TDR [1].

In this third method of determining the rt-relation the so-called auto-calibration method was used [22, 23]. The method is based on the assumption that the track parameters resulting from a fit will provide a better estimate of the distance between a track and the wire, compared to the estimate from the hits themselves. The tracks are used to predict the distance r_i. The difference between the reconstructed time $t(r_i)$ and the measured time t_i is then minimized to obtain $t(r_i)$. The track fit was performed by minimization of the χ^2, determined as

$$\chi^2 = \sum_{i=1}^{N_{hits}} \frac{(\tau_i - t(r_i))^2}{\sigma_t^2(r_i)}, \tag{4}$$

where N_{hits} is the number of hits used in the track fit, τ_i is the measured drift time of hit i, r_i is the distance between the track and the wire at which the hit i occured, $t(r)$ and $\sigma_t(r)$ are the tr-relation and time resolution functions which were determined iteratively. The rt-relation is simply the inverse function of $t(r)$. The resulting χ^2-distribution is shown in Fig. 13.

A hit was used for the track reconstruction if the drift time was in agreement with the track prediction within $6\sigma_t$. Only those tracks were kept which had at least 4 hits and and had a length along the beam direction of at least 150 mm. The event was used for subsequent analysis if it contained precisely one track, which rejected 5–7% of the events.

The rt-relation as obtained by either of the three analyses are in good agreement, as will be shown in Sections 4.4 and 6.

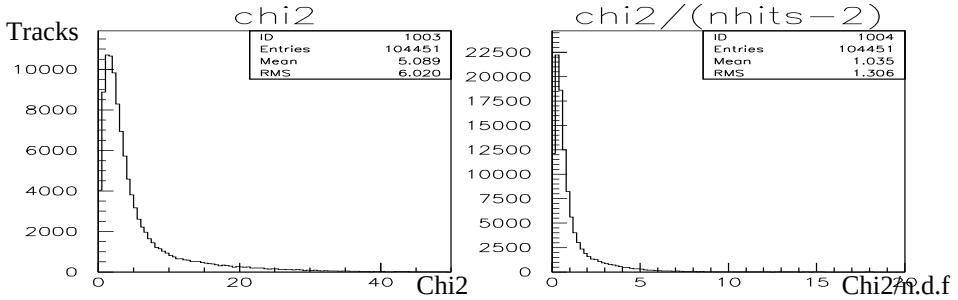

Figure 13: *Both the χ^2 distribution and the χ^2/n.d.f of the OT tracks is shown. The average χ^2/n.d.f is close to unity, indicating that the errors were estimated properly.*

4.4 Study of OT position measurement performance

In both approaches, with the Si-telescope and with OT information standalone, the coordinate resolution was determined from the distribution of the track residuals, i.e. from the differences between the measured coordinates in the detector and those predicted according to reconstructed track parameters. For the conversion of measured drift time into distance to the wire the inverse of the tr-relation was used.

In the study where the Si-telescope was used, the $t(r)$ relations was determined from the correlation between the measured drift time and the predicted track distance to the wire, see Appendix A.1, whereas in the OT standalone analysis it was obtained from an iterative calibration procedure, see Sec-

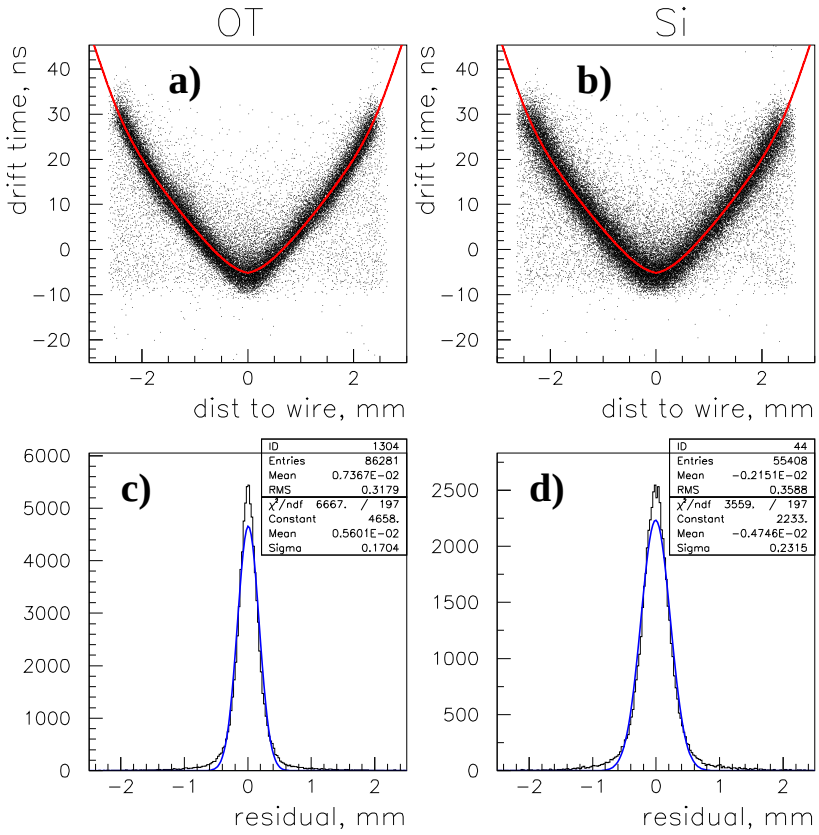

Figure 14: *The correlation between the OT drift time and the track distance to the wire is shown, as determined with OT standalone (a) and by using the Si-telescope (b). The superimposed curve is the fitted tr-relation (see Section 4.3). The corresponding distributions of the track residuals are also shown (c), (d).*

tions 4.2 and 4.3. The final values for the resolution were obtained from the width of a gaussian fit to the residual distributions. Differences in the resolution when only the core of the residual is fitted, or when a double gaussian was used, are quantifed in Appendix A.1. Note also that the coordinate resolution depends significantly on the distance between track and wire, see Appendix A.3.

Figs. 14*a,b* show the correlation between the OT drift time and track distance to the wire for plane 3 in a run in which the Si-telescope information was available and all the OT modules were operated at HV=1580 V, U_{thr}=700 mV. The track reconstruction was performed using the OT data, with plane 3 excluded from the track fit (Fig. 14*a*) and using the Si-telescope data (Fig. 14*b*), respectively. In Fig. 14*c, d* the corresponding distributions of the track residuals and the superimposed gaussian fits are shown.

4.4.1 Correction for track bias of residual

In the OT standalone analysis the resolution values obtained from the track residuals are biased. If the hits of the plane under study are excluded from the track fit, the variance of residuals overestimates the resolution, because of the finite precision of the track parameter reconstruction in the other OT planes. On the other hand, if the hits of the plane are included in the fit,

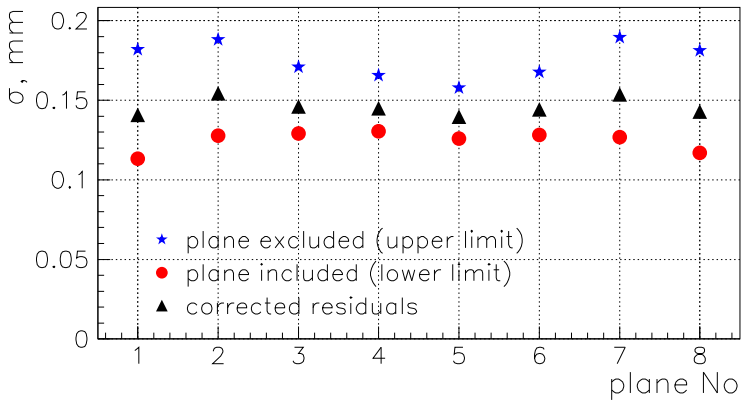

Figure 15: *The resolution studies in the OT standalone analysis. The resolution values for the eight planes were obtained from track residuals for hits included into the track fit (underestimated), excluded from the fit (overestimated) and with correction applied. The data of run 1322 are used, with HV=1600 V and* U_{thr} = 700 *mV. See Section 4.3 for details of the analysis.*

the variance of residuals for this plane underestimates the true resolution. In particular, the resolution of 170 μm obtained from the fit to the residual distribution in Fig. 14*c* is overestimated, because plane 3 was excluded from the track fit. In order to obtain an unbiased estimate of resolution, an event-by-event correction was applied based on the covariance matrix of the track parameters [23]. In the remainder of this note, the values of the resolution determined with the OT standalone analysis are obtained with this correction.

The size of over- and underestimation for each of the eight planes of the OT modules is shown in Fig. 15, for HV=1600V. Numerical values for the resolution at HV=1550V are given in Table 1. The residuals in the outer planes are larger due to the larger uncertainty in the track prediction. After correcting the residual for the uncertainty in the track prediction, approximately equal resolution is obtained for all layers.

layer	intrinsic resolution (μm)	measured residual (μm)	error track prediction (μm)
1	168	201	110
2	166	197	106
3	158	175	75
4	159	175	73
5	154	170	72
6	146	164	74
7	157	190	107
8	157	193	112

Table 1: *Resolution for each layer at HV=1550V, $U_{thr} = 700$ mV, including the correction from the error on the track prediction. The measured resolution is obtained from a gaussian fit to the residual around $\pm 2\sigma$ around the mean. See Section 4.2 for details of the analysis.*

4.4.2 Multiple scattering of Si-tracks

The resolution obtained from the residual distribution when using the Si-tracks (Fig. 14*d*) is overestimated. The multiple scattering in the Si-detector planes, and for part of the runs also in the scintillator S3, smear the distribution of the predicted hit position.

The multiple scattering was studied in two ways. The coordinate resolutions for each OT detector plane as obtained with the Si-tracks and with the OT standalone analysis were compared. Secondly, runs were taken at different beam energies, so that the multiple scattering contribution could be extracted from the energy dependence.

The result of the comparison of the Si and OT standalone resolutions is shown in Fig. 16*a*. The horizontal axis represents the z-coordinate (along the beam), where the z-position of the OT and Si-planes are indicated. The difference between the two estimates increases with z. The multiple scattering contribution, $\sigma_{MS} = \sqrt{\sigma_{Si}^2 - \sigma_{OT}^2}$, is shown in Fig. 16*b*. The straight line fit to the points is superimposed on the plot. As expected, the main multiple scattering contribution effectively comes from the last Si-plane: the scattering in the first two planes is absorbed by the procedure of the track fit in the telescope. The multiple scattering amounts to about 0.3 mrad.

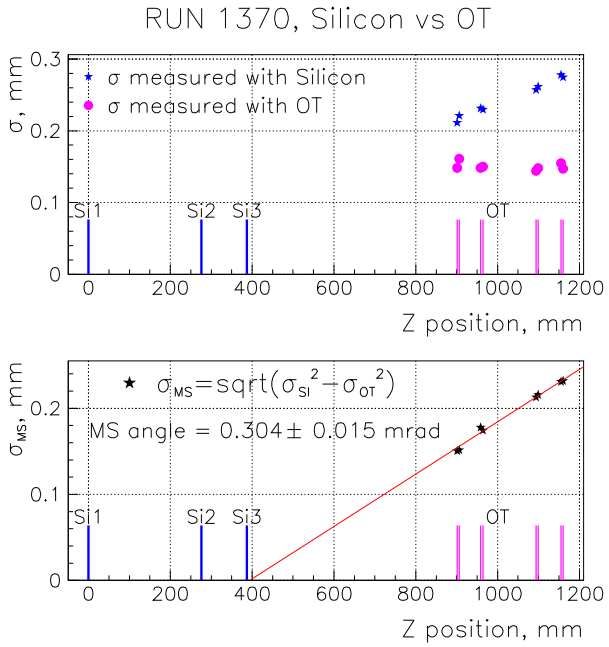

Figure 16: *Resolutions of each OT plane estimated with Si and OT as a function of its z position (a); multiple scattering contribution* ($\sigma_{MS} = \sqrt{\sigma_{Si}^2 - \sigma_{OT}^2}$) *(b).*

$\sigma_{\text{MS, 6GeV}}$		without S3		with S3	
		(μm)	(mrad)	(μm)	(mrad)
Module 2	plane 3,4	143	0.253	195	0.345
Module 3	plane 5,6	176	0.249	246	0.348

Table 2: *The contribution to the residual as a result from multiple scattering are estimated from the energy dependence of the residual, see Fig. 17. Both the contribution to the residual (dependent on the z-position of the modules) and the angular spread are given.*

Alternatively, the amount of multiple scattering was estimated by running at different beam energies. The resolution was measured with and without the scintillator S3 between the silicon sensors and the OT. The results are given in the table below, and are consistent with the value from Fig. 16*b*. These values were used to correct the residuals in order to obtain the resolution.

After the corrections described above, the Si and OT analyses are compatible, and the results obtained with both of the techniques are presented in this note.

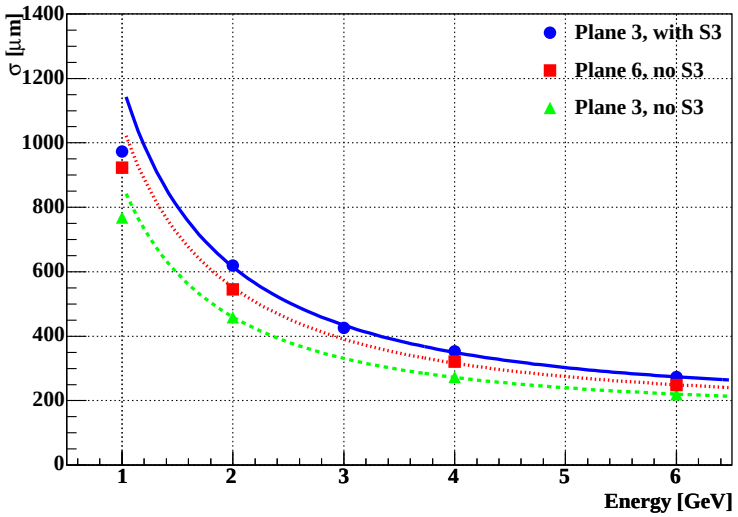

Figure 17: *Resolutions of the OT as measured at 1600 V and 700 mV using the Si-tracks, as a function of the beam energy. The line indicates the fit using* $\sigma_{tot} = \sqrt{\sigma_{OT}^2 + (\sigma_{MS,1GeV}/E)^2}$. *The point at 1 GeV is not used in the fit.*

4.5 Noise

The fake hits produced by the electronic noise were studied with a random trigger at several settings of the ASDBLR discriminator threshold. The measured quantity is the average noise occupancy R in each frontend module, defined as the average number of hits per channel per event:

$$R = \frac{\sum_{\text{evts}} \sum_{\text{ch}} \text{hit}}{N_{\text{evts}} N_{\text{ch}}}. \tag{5}$$

The average noise occupancy R is related to the noise hit rate per wire f as $R = f \cdot 75$ ns. The measured dependence of the noise on the amplifier threshold will be shown in Fig. 21 in Section 6.

4.6 Cross talk

The cross talk is a consequence of electromagnetic coupling between neighbouring channels. Its intensity can be defined as the probability that, if straw i produces a hit caused by the particle, either of the neighbouring straws also produces a hit:

$$\text{crosstalk}_\text{i} = \frac{N_{i-1} + N_{i+1}}{N_i}. \tag{6}$$

The strength of crosstalk is an important parameter for the choice of the working point of the OT detector.

The hit distribution for plane 3 is shown in Fig. 18*a* for those events in which the track points to wire 41 *and* there is a hit in this wire that

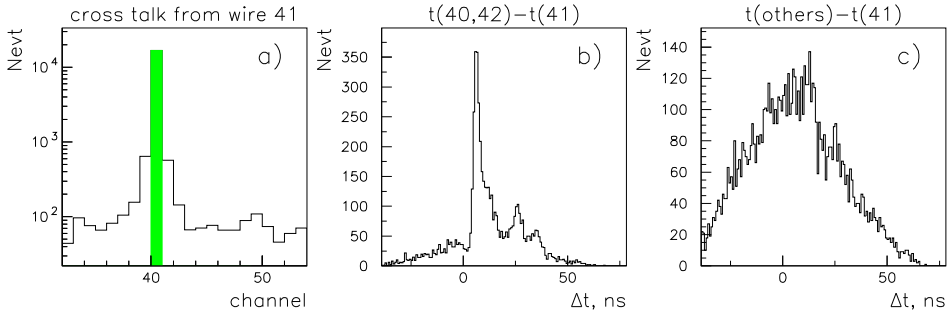

Figure 18: *The straw hit map (a) is shown for those tracks that point to straw 41. The time difference distributions for neighbouring (b) and non-neighbouring (c) channels show that hits in neghbouring channels mainly come from crosstalk, while in other channels they are mostly noise. This data was taken at HV=1700 V.*

is compatible with the track. The high voltage at plane 3 in this run was 1700 V. The time difference between the crosstalk hits in channels 40 and 42 and the track hit in channel 41 is shown in Fig. 18*b*. The time correlation is evident, which is a clear signature of cross talk. The distribution of the time difference for other (non-neighbouring) channels is shown in Fig18*c*, indicating random noise.

The correction for random noise on the cross talk estimate was done by subtracting the average probability to have a hit in non-neighbouring channels.

4.7 Efficiency

The efficiency is the probability that a hit is observed if a charged particle traverses the detector. For a reliable determination of the efficiency, the predicted position of the hit is obtained from reconstructed tracks. The track reconstruction can be performed either with the Si-telescope or with the OT itself. In the latter case the layer(s) for which the efficiency is determined were excluded from the track reconstruction. The efficiency can be estimated as the ratio of the number of observed hits to the number of expected hits in the detector.

The efficiency profile along a OT module is not uniform. The efficiency inside a straw drops at the edges of the straw, and is fully inefficient in the gap between two neighbouring straws. In order to show the dependence of the efficiency on the HV or amplifier threshold, a single number is desireable. Several definitions can be made.

4.7.1 Average efficiency

The efficiency can simply be defined as the number of valid hits in the OT divided by the total number of tracks. Only the hits in those straws are considered, where the tracks point to, or in one of the two neighbours. The efficiency was averaged over all irradiated straws in a given plane, resulting in the so-called layer-efficiency ϵ_{layer}:

$$\epsilon_{\text{layer}} = \frac{N_{hit}}{N_{track}}, \tag{7}$$

where N_{track} is the number of tracks under study (see Section 4.3), and N_{hit} is the number of events in which a hit occured in either the straw where the track points to or in one of the two straws next to it. The track parameters were estimated using the remaining 7 planes of the OT.

However, the geometry of one OT plane results in a certain amount of dead area. The inner diameter of a straw is 4.9 mm, whereas the pitch between the straws is 5.25 mm. The fraction of active area of one OT monolayer hence amounts to $\frac{4.90}{5.25} \approx 93.3\%$.

By correcting for the dead area between two straws, the average cell-efficiency is obtained:

$$\epsilon_{\text{cell}} = \epsilon_{\text{layer}} \cdot g \ , \tag{8}$$

where g is the geometrical factor which is equal to the ratio of the wire pitch to the straw inner diameter: $g = \frac{5.25}{4.90} \approx 1.071$.

Note that the efficiency estimated in this way is based on the nominal value of the straw inner diameter and can be biased if the actual diameter differs from its nominal value (a tolerance of $\pm 50\mu$m as given by the producer *Lamina* translates into a variation of $\pm 1\%$) or in case of slight deformation of the straws during the assembly. Additionally, the small beam width could result in an erroneous estimation of the *fraction* of dead area between the straws, since the runs with the Si-telescope have an illuminated width of only 9 mm. The average efficiency measurements are expected to have up to $\sim 2\%$ systematic uncertainty because of the geometrical factor. This does however not affect the determination of the plateau position.

Finally, the average efficiency is corrected for random noise, using $\epsilon_{meas} = \epsilon_{true} + (1 - \epsilon_{true})R$, where R is the noise probability. For reasonably low noise ($<1\%$) and high efficiency ($>90\%$) this correction can savely be neglected.

4.7.2 Plateau efficiency

Alternatively, the efficiency can be evaluated by its plateau value in the center of the straw, within $|r| < 1.6$ mm from the wire. This window is enlarged to 2.0 mm for the OT standalone analysis, that does not suffer from multiple scattering effects. Ideally, the efficiency can be modeled as follows. In a gas mixture of Ar/CO_2-70/30 the average ionisation length λ amounts to about 325 μm [19]. As a result, the probability to create a cluster is smaller at the edges of the straw, where the path length of the particle through the straw is limited. Using Poisson statistics the cell-efficiency as a function of the distance to the wire, X, can be estimated as:

$$\epsilon_{\text{cell}}(X) = \epsilon_{\text{plateau}}\Big(1 - e^{-2\sqrt{R^2 - X^2}/\lambda}\Big), \tag{9}$$

where R is the radius of the straw (2.45 mm) and X the distance to the wire. Statistically this results in an integrated efficiency loss of 0.5%.

The plateau efficiency can in principle deviate from unity due to fluctuations in the gain of the avalanche.

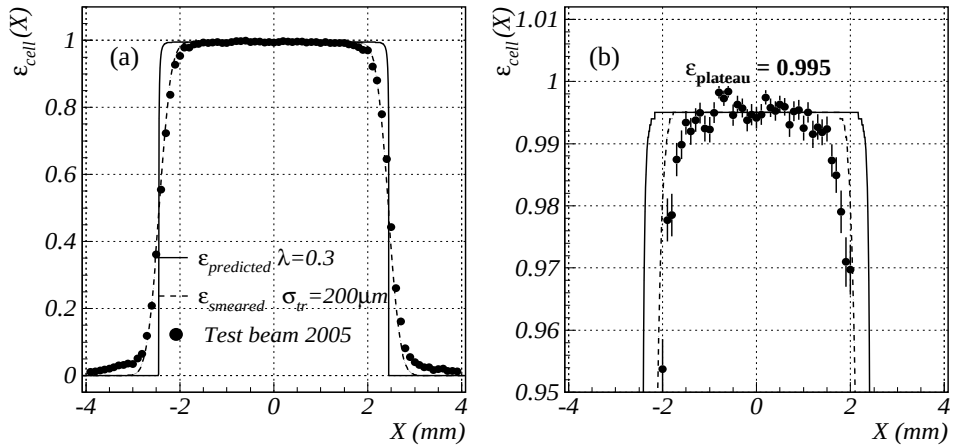

Figure 19: *The straw efficiency profile is shown, as obtained with the analysis described in Section 4.1, averaged over module 2 and 3 at HV=1600 V and* $U_{thr} = 700$ *mV. (a) The drop in efficiency at the sides is caused by the finite Si-track resolution, see Section 4.4.2. (b) A zoom-in to the plateau region reveals an efficiency of >99% in the region* ± 1.6 *mm.*

The efficiency profile is shown in Figs. 19 and 20. The profile as obtained using the Si-track prediction (Fig. 19) is distorted at the edges due to the imperfect track prediction. The position of the track is smeared due to the multiple scattering in the last Si-station, see Section 4.4.2, as shown by the dashed line. The predicted efficiency from Eq. (9) is shown by the full line.

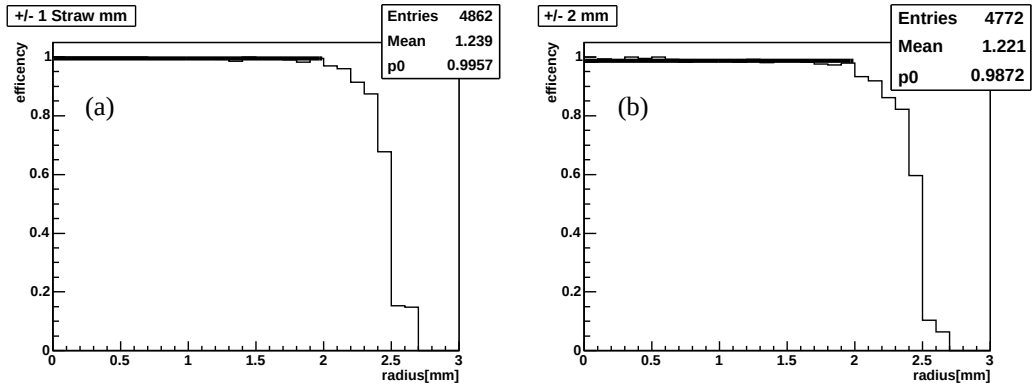

Figure 20: *The straw efficiency profile of layer 5 (mod 3) at HV=1550V,* $U_{thr} = 700$ *mV (run 316) is shown for the OT standalone analysis (Section 4.2), as a function of the predicted track position. The sharp drop at* ~ 1.6 *mm is absent, because the track prediction is not diluted by multiple scattering. (a) The efficiency plateau is shown, where the detector is defined to be efficient if a hit is found in the predicted straw, or in either neighbour. (b) The hit is counted in the efficiency only if it is consistent with the track within 2.0 mm.*

5 Available Data Sets

The performance of the OT modules was studied when varying the high voltage and the ASDBLR threshold voltage around their nominal values. For the measurements without the Si-telescope, the parameters were varied only in plane 3, while keeping the other planes at nominal values HV=1580 V and U_{thr}=700 mV, in order to provide good track reconstruction. In the runs with the Si-telescope, the parameters in the planes 3–6 were varied simultaneously.

The OT modules were installed on a vertically moveable support, in order to be able to vary the position of the beam spot along the wire upto a range of 45 cm. Measurements were done at two vertical positions of the chambers, one with the beam spot near the end of the wires and another at 45 cm from the end. These positions will be referred to as "high" and "low", respectively. The OT modules 1, 3 and 4 were installed with the frontend electronics box up, and module 2 with the electronics box down, see Fig. 2. Module 2 was thus studied at distances y=0 and 45 cm from the preamplifiers, while the frontend electronics for the other modules were at a distance from the beam spot of y=225 and 180 cm, respectively, in the "high" and "low" positions.

The data sets used in the analysis are given in Table 3, below.

Runs	Meas.	Figure	OT pos.	U_{thr} (mV)	HV (V)	Si-tel.	S3	E (GeV)
301-359	thresh. scan	25	high	400-1540	1550	no	yes	6
1201-1219	hv scan		high	700	1300-1700	yes	yes	6
1230-1243	thresh. scan		high	575-900	1550	yes	yes	6
1263-1277	energy scan	17	high	700	1600	yes	yes	1-5
1279-1283	energy scan	17	high	700	1600	yes	no	1-5
1286-1312	hv scan	22b, 23b	high	700	1300-1700	yes	no	6
1320-1330	hv scan	22a,23a,24	high	700	1200-1700	no	no	6
1331-1341	hv scan	22a,23a,24	low	700	1200-1700	no	no	6
1342-1351	hv scan	22a,23a,24	low	800	1200-1700	no	no	6
1362-1368	noise	21	low	645-800	1580	no	no	6
1370			low	700	1580	yes	no	6

Table 3: *Available data sets. Note that the HV and the amplifier threshold of the 1^{st} and 4^{th} module is always at 1580 V and 700 mV, respectively.*

6 Results

The average noise frequency per wire f as a function of the ASDBLR threshold is shown in Fig. 21. The corresponding scale for the noise occupancy, $R = f \cdot 75$ ns, are given at the right of the plot. The first module shows somewhat lower noise rate than the other three. Note that the typical occupancy of a B-event is around 4%. An additonal occupancy of 0.1% at thresholds higher than 700 mV does not affect the track reconstruction performance [24].

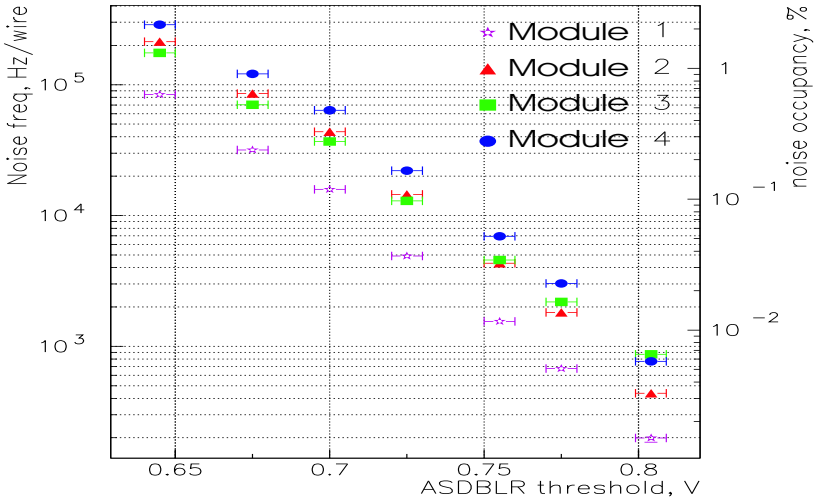

Figure 21: *The average noise frequency in Hz/wire for the 4 modules. The corresponding values of noise occupancy are given at the right.*

The efficiency curves as a function of the applied high voltage, taken at various ASDBLR threshold settings and various beam positions, are shown in Fig. 22. The efficiency at the far end, with beam spot at 225 cm from the preamplifiers, corresponds to the data from module 3. The efficiency is higher than at the near end (0 and 45 cm) from module 2 taken at the same threshold. This is in agreement with the fact that the signal amplitude from the far end is higher because of the superimposition of direct and reflected signals [25].

As expected, the efficiency curve for the higher threshold of 800 mV undershoots the curve of 700 mV. The average cell efficiency as obtained with the OT standalone analysis differs from the plateau efficiency as obtained by the Si analysis by $\sim 0.5\%$.

In general, the OT detector reaches full efficiency at 1550 V, independent of the amplifier threshold settings, or beam spot position.

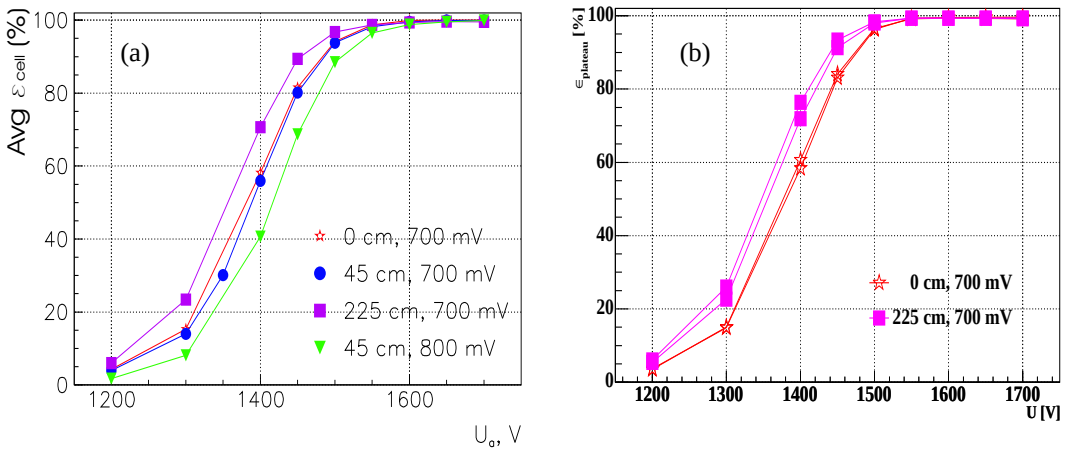

Figure 22: *The efficiency dependencies on HV at various beam positions and ASDBLR thresholds. Both the average cell efficiency (a) and the plateau efficiency is shown (b). The double curves in (b) show the results of both planes separately.*

The corresponding coordinate resolution as a function of the HV is shown in Fig. 23, corrected for the track uncertainty or the multiple scattering, respectively. The resolution is dependent on the method with which the rt-relation is obtained, see Sections 4.1-4.3. At HV=1400 V the resolution for plane 3 and 4 is very large, due to the non-gaussian distribution of the residual. Large tails make the single-gaussian fit unstable. The variation of the resolution for alternative fits of the residual is discussed in the Appendix A.2. Nevertheless, the detector resolution is better than the design value of 200 μm at high voltages above 1550 V for both methods [3].

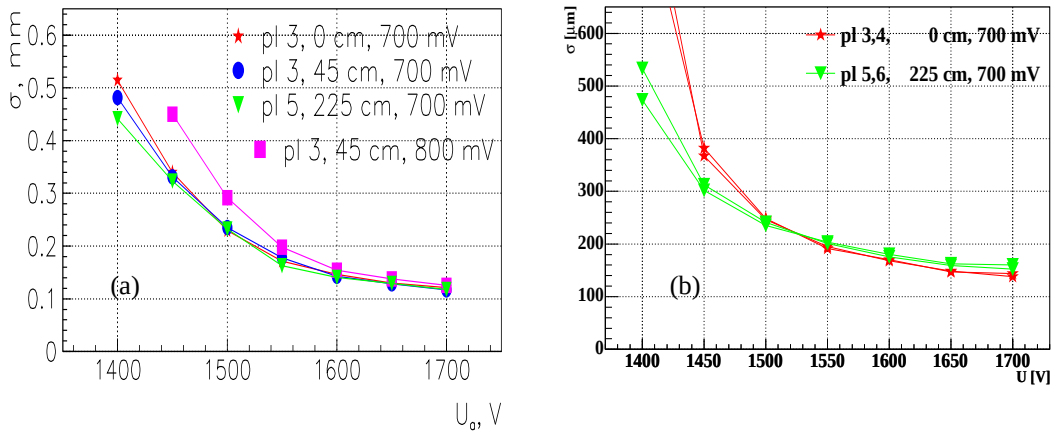

Figure 23: *The coordinate resolution as a function of HV at various beam positions and ASDBLR thresholds.*

[3]The drift cell parameters obtained from the calibration procedure for high voltage of 1600 V and threshold of 800 mV at beam position of 45 cm are given in the Appendix A.3.

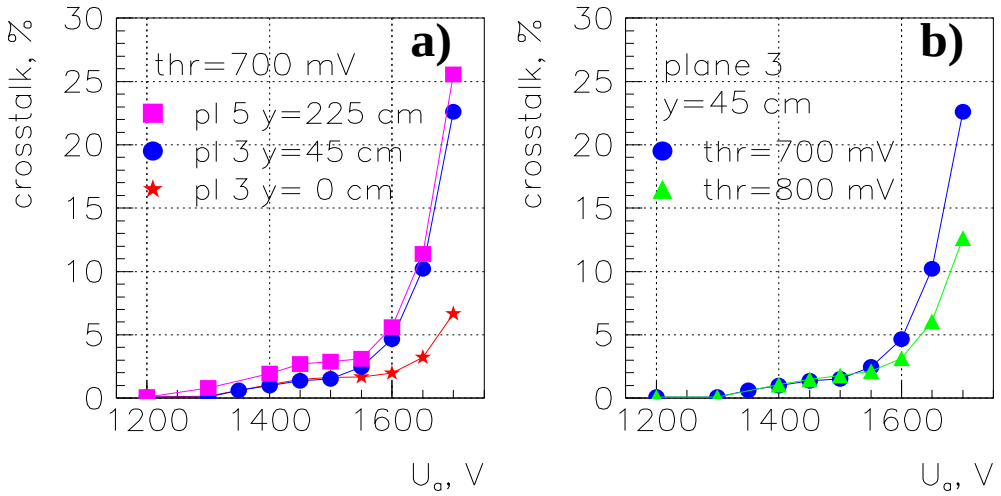

Figure 24: *The cross talk as a function of HV: ASDBLR threshold of 700 mV, beam at 0, 45 and 225 cm (a); ASDBLR thresholds of 700 and 800 mV, beam at 45 cm (b)*

The crosstalk dependencies on HV at the ASDBLR threshold of 700 mV and various beam positions are shown in Fig. 24*a*. The crosstalk is minimal when the beam spot is close to the readout end and significantly grows towards the far end. The crosstalk can be suppressed significantly by increasing the threshold to 800 mV, as is shown in Fig. 24*b*. The crosstalk level is acceptable (<10%) at high voltages below 1650 V.

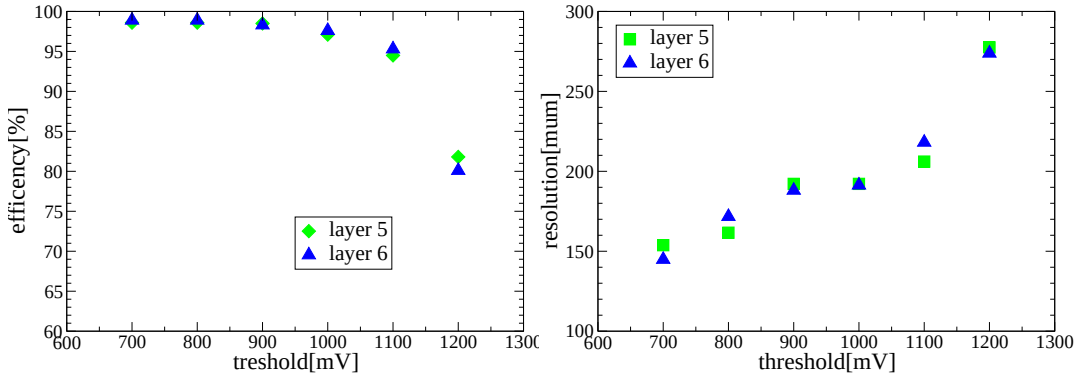

Figure 25: *The dependence of efficiency (a) and resolution (b) on ASDBLR threshold for module 3 (planes 5 and 6) at HV=1550 V. Note that the resolution is obtained from a fit to the residual in a range of $\pm 2\sigma$, resulting in slightly better resolutions, see Section A.2*

.

The crosstalk between the two *planes* of module 2 was studied by setting the high voltage of one of the planes to zero and varying the high voltage of the other plane. It was found that at high voltages up to 1700 V the crosstalk between planes does not exceed 1%.

The dependencies of efficiency and resolution for modules 2 and 3 (planes 3–6) on the ASDBLR threshold at HV=1550 V is shown in Fig. 25. The OT detector performance does not strongly depend on the ASDBLR threshold in the range around 700–800 mV, corresponding to 3–4 fC. The crosstalk at this voltage was found to be <4% for all thresholds.

Finally, the effect of the length of the readout window on the efficiency is studied. By cutting part of the TDC spectrum, hits may be lost. By cutting at 45 ns the efficiency gets reduced by a relative 2%, see Fig. 26.

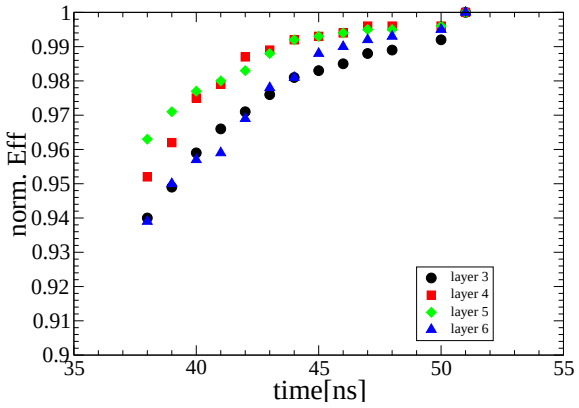

Figure 26: *The dependence of efficiency as a function of OTIS time window, at HV=1550 V.*

7 Conclusions

The beam test with 6 GeV electrons of four S-type OT modules with final prototype frontend electronics has demonstrated good OT detector performance. For an example setting of the parameters at HV=1550 V and amplifier threshold at 800 mV the following key performance numbers can be quoted:

- high efficiency ($\sim 98\%$);
- coordinate resolution better than 200 μm;
- acceptable noise (< 10 kHz/wire) and crosstalk level ($< 4\%$).

These results are confirmed by three different, independent analyses, using different methods.

Within the threshold range of 700–800 mV and high voltage range between 1520–1650 V the detector performance meets the design requirements with efficiencies higher than 95% and resolution better than 200 μm with reasonable noise and crosstalk level.

The tracking performance in terms of efficiency and ghost rate as a function of the OT tracker resolution and cell-efficiency goes beyond the scpoe of this note and can be found elsewhere [24].

A rt-relation

A.1 Parabolic parametrization

The rt-relation as used in the Si-analysis - as described in Section 4.1 - was obtained by fitting a second order polynomial to the relation between drift time and predicted track position, see Fig. 27. The 2d-t(r) histogram was sliced in bins of the predicted track position, and subsequently the mean drift time was determined with a gaussian fit around 2σ of the peak. The final t(r)-relation was determined with the fit through the mean drift times per slice, given by:

$$\begin{aligned} t(r) &= p_0 + p_1(r - p_2)^2 \quad \text{for } r < 0 \\ t(r) &= p_0 + p_1(r - p_3)^2 \quad \text{for } r > 0, \end{aligned} \tag{10}$$

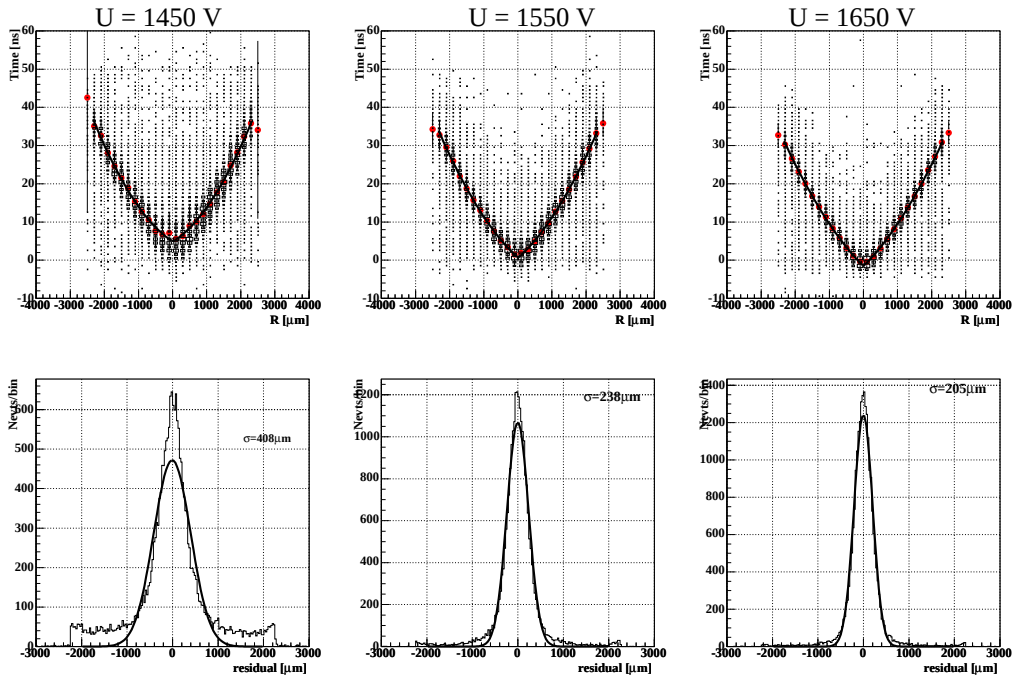

Figure 27: *The rt-relation and the resulting coordinate resolution is shown for three values of the applied high voltage. Note that this is the raw residual, not corrected for multiple scattering in the last silicon plane, see Section 4.4.2.*

U (V)	t_0 (ns)	r_{wire} (μm)	p_0	p_1	p_2	p_3
1450	4.2	16	1.0	0.33E-05	-974	1007
1550	0.8	13	-4.5	0.28E-05	-1356	1382
1650	-1.3	2	-8.4	0.24E-05	-1708	1712

Table 4: *The $t(r)$ parameters as obtained from the fit of Eq. (10).*

which is a half parabola, mirrored at the wire position $r_{\text{wire}} = (p_2 + p_3)/2$. The (arbitrary) time offset t_0 can be obtained through:

$$t_0 = p_0 + p_1\Big(\frac{p_2 - p_3}{2}\Big)^2. \tag{11}$$

The values for p_{0-3}, are given in Table A.1. The parameters p_2 and p_3 are very similar by construction, because the plots were constructed such that the wire position was set at $r = 0$.

A.2 Fit of the residual

The coordinate resolution is obtained by fitting a gaussian to the residual. However, as is seen in Fig. 27, in some cases the residual is not well described by a gaussian distribution, due to the presence of large tails, presumably caused by the fact that the hit is not due to the *first* cluster.

To show the affect on the resolution, both the results from a gaussian fit around the core of the residual within $\pm 1.5\sigma$, as well as from a double gaussian fit are presented, see Fig. 28, using $\sigma_{\text{double gaussian}} \equiv \frac{c_1\sigma_1 + c_2\sigma_2}{c_1 + c_2}$.

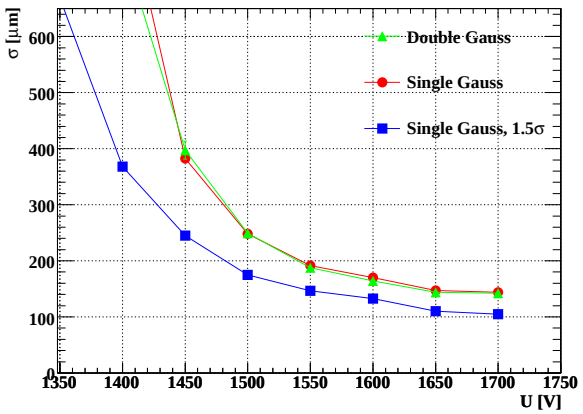

Figure 28: *The resolution is plotted for plane 3, with different definitions of the resolution, depending on the fit to the residual distribution.*

A.3 Resolution vs distance to wire

The drift time $t(r)$ and time resolution $\sigma_t(r)$ as a functions of distance between track and wire are shown in Fig.29a and b, respectively. Fig. 29c shows the coordinate resolution as a function of drift distance estimated using the error propagation formula,

$$\sigma_r(r) = \frac{\sigma_t(r)}{dt(r)/dr}.$$

One can see that the drift time resolution at this high voltage is almost independent on drift distance; the significant non-uniformity of coordinate resolution appears because of the non-linearity of the tr-relation (drift velocity is not saturated).

In the analysis procedure, the $t(r)$ and $\sigma_t(r)$ functions were represented by their values in several fixed points on r; the values in the intermediate points were obtained using the interpolation with 3^{rd} degree B-splines (CERNLIB E210). For future reference, the functions' values in these fixed points are given in Table 5, for HV=1600 V, U_{thr} = 800 mV and Ar/CO_2=70/30.

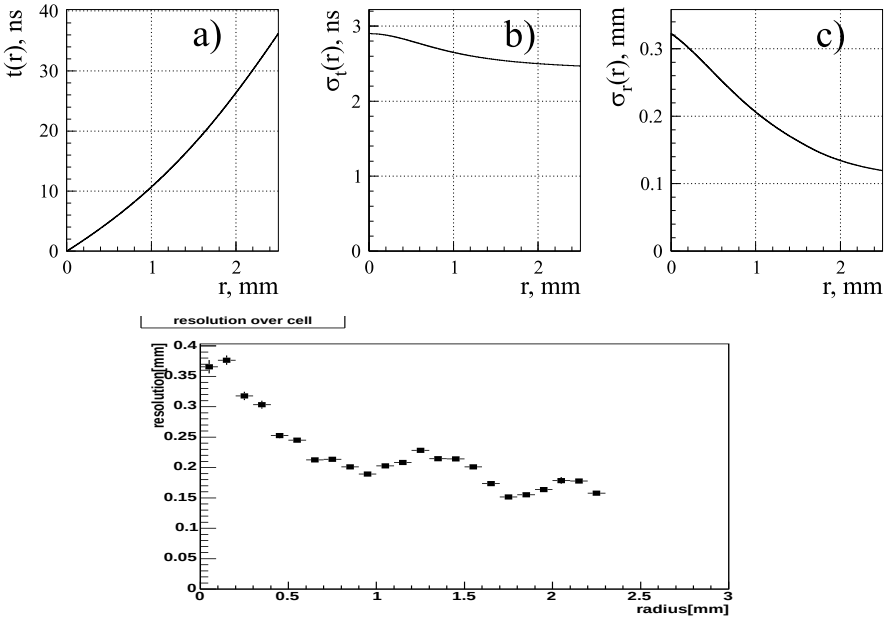

Figure 29: *The tr-relation (a) and time resolution (b) as a function of distance to the wire for HV=1600 V, thr=800 mV at beam position of 45 cm; the coordinate resolution estimated in the linear approximation (c). The lower plot shows the measured resolution at HV=1550 V, U_{thr} = 700 mV, with the residuals fitted at the core of $\pm 2\sigma$.*

r, mm	t, ns	σ_t, ns
0	0	2.929
0.5	4.851	2.828
1.0	10.68	2.676
1.5	17.78	2.579
2.0	26.37	2.525
2.5	36.23	2.493

Table 5: Values of $t(r)$ and $\sigma_t(r)$ for Ar/CO_2=70/30, HV=1600 V and U_{thr}=800 mV.

References

[1] The LHCb Collaboration, P.R.Barbosa et al., *Outer Tracker Techical Design Report*, CERN/LHCC 2001-024, Sep 2001.

[2] I. Gouz, B. Hommels and G.W. van Apeldoorn, *Beam tests of LHCb Outer Tracker prototypes in 2000*, LHCb-2001-011, Feb 2001.
I. Gouz, Th.Bauer and B. Hommels, *Beam tests of a full-scale prototype of the LHCb Outer Tracker straw tube modules*, LHCb-2001-098, Jul 2001.

[3] A. Berkien, H. Deppe, A. Pellegrino, T. Sluijk, U. Stange, U. Trunk, U. Uwer, D. Wiedner, A. Zwart, *The LHCb Outer Tracker Front End Electronics*, to be published as LHCb note.

[4] M. Moritz, *Measurement of the High Q^2 Neutral Current DIS Cross Section at HERA*, PhD thesis, p. 34, Hamburg, December 2001;
I.R. Fernadez, *Charm production at HERA*, PhD thesis, p. 109, Madrid, May 2001.

[5] N. Dressnandt et al., *Implementation of the ASDBLR Straw Tube Readout ASIC in DMILL Technology*, IEEE (2000) Trans. on Nucl. Sci. **48** n4, 1239, 2000,
R. Bevensee et al., *An Amplifier-Shaper-Discriminator with Baseline Restoration for the ATLAS Transition Radiation Tracker*, IEEE (1996) Trans. on Nuc. Sci. **43**, 1725, 1996.
See: `http://www.hep.upenn.edu/atlas/asdblr`

[6] T.Sluijk and U.Uwer, *Specification of the OTIS-to-ASDBLR interface.*
See: `www.physi.uni-heidelberg.de/~uwer/lhcb/Electronics/Review/`

[7] H. Deppe, U. Stange, U. Trunk, U. Uwer, *The OTIS Reference Manual v1.1*, Feb 2004.
See: `www.physi.uni-heidelberg.de/~uwer/lhcb/Electronics/Review/`

[8] U. Stange, *Development and Characterization of a Rad Hard Readout Chip for the LHCb Outer Tracker Detector*, PhD Thesis, Uni Heidelberg, 2005.

[9] A.N.M. Zwart, *OTIS Board Version 1.0*, Aug 2003.
See: `www.nikhef.nl/pub/experiments/bfys/lhcb/outerTracker/Electronics/FE-Electronics/otisboard.html`

[10] P. Moreira, T. Toifl, A. Kluge, G. Cervelli, A. Marchioro, and J. Christiansen, *GOL Reference Manual, Gigabit Optical Link Transmitter manual*, Version 1.9, Oct 2005.
See: `http://proj-gol.web.cern.ch/proj-gol/`

[11] U. Uwer, D. Wiedner, A. Berkien, T. Sluijk, A. Zwart, *Specifications for the IF13-2 Prototype of the Auxiliary Board for the Outer Tracker*, LHCb-2005-039, Jul 2005.

[12] P. Moreira, *QPLL Manual: Quartz Crystal Based Phase-Locked-Loop for Jitter Filtering Application in LHC*, Version 1.0, Jan 2004.
See: `http://proj-qpll.web.cern.ch/proj-qpll/`

[13] G. Haefeli, U. Uwer, A. Vollhardt, D. Wiedner, *Prototype IF14-1 for an Optical 12 input Receiver Card for the LHCb TELL1 Board*, LHCb-2004-072, Sep 2004.

[14] Altera Corporation, *Stratix PCI Developement Board Data Sheet*, Version 2.0, Sep 2003.

[15] J. Knopf, *Aufbau eines Auslesesystems für die Äuseren Spurkammern des LHCb-Detektors*, Diploma Thesis, Physikalisches Institut Heidelberg, 2004.

[16] R. Jacobsson, *How can I run my detector? Readout Partitioning and Running Modes*, LHCb-2001-140, Nov 2001.

[17] R. Schwemmer, *User Interface for the TTC-VMEbus Interface TTCvi.*
See: `http://ttc.web.cern.ch/TTC/TTCmain.html#TTCvi`

[18] P. Moreira, *TTCrq Reference Manual, CERN-EP/MIC*, Version 1.0, Oct 2003.
See: `http://proj-qpll.web.cern.ch/proj-qpll/ttcrq.htm`

[19] F. Sauli, *Principles of Operation of Multiwire Proportional and Drift Chambers*, CERN-1977-9, p.9, May 1977.
See `https://uimon.cern.ch/twiki/bin/view/LHCb/LHCbOT/`

[20] R. van der Eijk, *Track reconstruction in the LHCb experiment* PhD Thesis University of Amsterdam, 2002, p.70
See `https://uimon.cern.ch/twiki/bin/view/LHCb/LHCbOT/`

[21] M. Deile and N.P. Hessey, *Obtaining the Space-Time Relationship of Drift Tubes from the Drift-Time Spectrum*, ATL-MUON-99-002, Apr 1999.
See `https://uimon.cern.ch/twiki/bin/view/LHCb/LHCbOT/`

[22] H. Tolsma, *The Honeycomb Strip Chamber: A two coordinate and high precision muon detector* PhD Thesis University Twente, 1996, p.75
See `https://uimon.cern.ch/twiki/bin/view/LHCb/LHCbOT/`

[23] W. Hulsbergen et al., *Calibration of HERA-B Outer Tracker Chambers in a Cosmic Ray Setup at NIKHEF*, HERA-B 00-014, Jan 2000.
See `https://uimon.cern.ch/twiki/bin/view/LHCb/LHCbOT/`

[24] M. Needham, *Tracking Performance and Robustness Tests*, LHCb-2003-020, 2003.

[25] Yu. Guz, G. van Apeldoorn, A. Pellegrino, T. Sluijk, A. Zwart, *Study of the Global Performance of an LHCb OT Front-End Electronics Prototype*, LHCb-2004-120, Jan 2005.